Journal of Applied Polymer Science

# Thermoresponsive hollow magnetic microspheres with hyperthermia and controlled release properties

**Lin Chen,[1,2] Huan Zhang,[1,2] Longfei Li,[1,3] Yongzhen Yang,[1,3] Xuguang Liu,[1,2] Bingshe Xu[1,3]**

[1]Key Laboratory of Interface Science and Engineering in Advanced Materials, Ministry of Education, Taiyuan University of Technology, Taiyuan 030024, China

[2]College of Chemistry and Chemical Engineering, Taiyuan University of Technology, Taiyuan 030024, China

[3]Research Center on Advanced Materials Science and Technology, Taiyuan University of Technology, Taiyuan 030024, China

Correspondence to: Y. Yang (E-mail: yyztyut@126.com) and X. Liu (E-mail: liuxuguang@tyut.edu.cn)

**ABSTRACT:** Thermoresponsive hollow magnetic microspheres consisting of a hollow magnetic core, a carbon shell, and a smart polymer layer are presented in this article. A carbon nanomaterial was used as a steric stabilizer for $Fe_3O_4$ nanoparticles and a supporter for polymer. The thermoresponsive monomer, *N*-isopropyl acrylamide, was grafted on the carbon-encapsulate hollows by surface radical polymerization. The experimental results indicate that the composites had a phase-transition temperature around 43°C and a saturation magnetization of 56.9 emu/g; this showed apparent thermosensitivity and magnetism. The performances in hyperthermia evaluated by an inductive magnetic field showed that the hybrid microspheres had a specific absorption rate of 240 W/g. The model drug, 5-fluorouracil, was loaded in and released from the microspheres with different release rates at 35 and 50°C. This demonstrated that the as-synthesized microspheres had a thermotriggered release ability and would be a good drug carrier in the biomedical field.
© 2015 Wiley Periodicals, Inc. J. Appl. Polym. Sci. **2015**, *132*, 42617.

**KEYWORDS:** composites; drug-delivery systems; functionalization of polymers; inorganic polymers; magnetism and magnetic properties

Received 7 April 2015; accepted 14 June 2015

**DOI: 10.1002/app.42617**

## INTRODUCTION

In past decades, thermoresponsive magnetic microspheres have emerged as a great potential technology platform for targeted and controlled drug delivery.[1–4] First, magnetic components can guide microspheres to lesions directly by an external magnetic field and release drug at the right place. Second, the thermoresponsive polymer shell acts as a drug carrier and swells or shrinks in response to temperature changes, realizing enhanced controlled release at the right time.[5] Moreover, magnetic nanoparticles (MNPs) accumulated in a tumor can also be used as a hyperthermia-inducing agent to raise the local temperature around the tumor site.[6] Therefore, typical thermoresponsive magnetic dual-responsive microspheres could realize the target, thermotriggered drug delivery, and hyperthermia simultaneously. These external stimuli-responsive characters offer obvious advantages of accurate spatial, temporal, and quantitative drug release through a remote apparatus, which is quite efficient and safe.[7]

Up to this point, a number of thermoresponsive magnetic systems have been developed. The most extensively investigated thermoresponsive polymer, poly(*N*-isopropyl acrylamide) (PNIPAM), has always been used as a polymer shell on the surface of MNPs to realize thermotriggered drug release because it has a phase-transformation temperature around 35°C, called the *lower critical solution temperature* (LCST), which is quite close to our body temperature. Laurenti *et al.*[8] and Purushotham and Ramanujan[9] described methods for the preparation of thermoresponsive microspheres with magnetic $Fe_3O_4$ cores separately. In both approaches, the $Fe_3O_4$ nanoparticles were synthesized, and their surface was subsequently modified and grafted with PNIPAM. One of the major drawbacks concomitant with this strategy is the easy coagulation of MNPs because of their own features. To prevent agglomeration, Rubio-Retama *et al.*[10] proposed an effective approach for preparing monodisperse thermoresponsive microspheres with MNPs decorated on their surfaces by an *in situ* method. However, the existence of the MNPs hampered the extension of PNIPAM segments and affected the efficacy of drug delivery. Therefore, Deng *et al.*[11] used $SiO_2$ as a stabilizer for MNPs to prepare dual-responsive microspheres with a core–shell structure.

Nevertheless, so far, most studies have focused on the solid core–shell hybrid microspheres. Few studies concerning

© 2015 Wiley Periodicals, Inc.

thermoresponsive magnetic microspheres with magnetic hollows have been reported. Hollow $Fe_3O_4$ magnetic spheres (HMSs) have attracted growing interest in a wide range of disciplines, including electrode materials,[12] magnetic resonance imaging,[13] drug delivery,[14] and hyperthermia.[15] It is convincing that the hollow interiors could be loaded with various cargoes, endowing the magnetic spheres with a variety of properties, such as fluorescence labeling.[16–18] Just like the solid core–shell thermoresponsive magnetic microspheres, it is crucial to propose strategies to chemically stabilize the MNPs against oxidation and agglomeration for preparing hollow magnetic ones.[19] In addition, the protection shell can also provide sites for further functionalization. These strategies include grafting of and modifying or coating with organic species, such as polymers and surfactants, or coating with inorganic materials, including silica and carbon. As we all know, the stability of polymers and surfactants is relatively low; for instance, they are irresistible to high temperature. Moreover, silica could not exist in an alkaline environment. Carbon nanomaterials, which have good mechanical, chemical, and thermal stabilities, stand out as coatings for core–shell structured composites and supporters for polymer layers. Our group has investigated carbon nanomaterials acting as PNIPAM supporters or encapsulating $Fe_3O_4$ nanoparticles in a previous study;[20] this verified that it is reasonable to choose carbon nanomaterials as a link bridge. In addition, composites incorporating carbon nanomaterials, such as PNIPAM with $Fe_3O_4$ nanoparticles, have been widely studied and used in the biological field. Substantial studies have demonstrated that they exhibit a low cytotoxicity.[21,22]

5-Fluorouracil (5-FU), a hydrophilic drug molecule, shows remarkable activity in inhibiting tumor growth. However, 5-FU has a high metabolism rate *in vivo* and can be easily absorbed into the blood; this leads to a low efficiency. Moreover, 5-FU has high toxic side effects in the body and could increase the risk of toxic injury when a certain amount of is 5-FU accumulated.[23] Although the incidence of side effects can be reduced by drug-delivery systems, an unsatisfactory 5-FU loading and controlled release efficiency have been reported.[24,25] Therefore, the development of a suitable drug carrier to control the release of 5-FU is imperative.

In this study, to enlarge the potential application of magnetic thermosensitive microspheres in the targeted drug-delivery system, hollow magnetic microspheres were introduced by the solvothermal method. Glucose was taken as the carbon source to encapsulate the magnetic hollow core and realize space stabilization.[26] Subsequently, carbon–carbon double bonds were introduced onto the surface of carbon-coated magnetite cores by 3-(trimethoxysilyl)propyl methacrylate (MPS). A thermosensitive monomer, *N*-isopropyl acrylamide (NIPAM), was grafted on the surface of the modified carbon-coated magnetic hollow microspheres. The products from different stages were designated as hollow magnetic spheres (HMSs), hollow $Fe_3O_4$/Carbon magnetic spheres (CHMSs), silanized hollow $Fe_3O_4$/carbon magnetic spheres (SCHMSs), and silanized hollow $Fe_3O_4$/carbon/poly(*N*-isopropyl acrylamide) magnetic spheres (TSCHMSs), as labeled in Figure 1. Finally, applications in hyperthermia, the 5-FU loading, and the controlled release behavior of the multifunctional microspheres were investigated.

## EXPERIMENTAL

### Materials

Anhydrous ferric chloride was purchased from Alfa Aesar. NIPAM, 5-FU, *N,N′*-methylene bisacrylamide, and phosphate-buffered saline (PBS) were purchased from Sinopharm Chemical Reagent Co. PNIPAM was synthesized according to previous literature.[27] Poly(vinyl pyrrolidone) (molecular weight = 30,000) and ethylene glycol were obtained from Tianjin Dengfeng Chemical Reagent Factory (China). Glucose monohydrate, trihydrate sodium acetate, potassium persulfate, and MPS were purchased from Tianjin Dongli Chemical Reagent Factory (China). Ethanol and nitric acid were obtained from Tianjin Guangfu Chemical Reagent Factory (China). All of the reagents were used without further purification. Distilled water was used in all of the experiments.

### Preparation of the HMSs, CHMSs, and SCHMSs

First, the HMSs were synthesized by a modified solvothermal reaction, as previously reported.[18] Briefly, 0.27 g of ferric chloride and 3.6 g of polyvinylpyrrolidone were dissolved in 70 mL of ethylene glycol with magnetic stirring until a light yellow solution formed. Then, 1.38 g of trihydrate sodium acetate was added and dissolved for 15 min under sonication. After that, the mixture was heated to 200°C and held at 200°C for 16 h in a 100-mL autoclave. The black products were collected by a magnet, washed with water several times, and dried.

Subsequently, 0.2 g of the HMSs was sonicated in a 0.1*M* nitric acid solution for 15 min and then rinsed to neutral. The treated microspheres were redispersed in 50 mL of water, and 4.95 g of glucose monohydrate was added with another 15 min of sonication. The solution was maintained at 180°C for 4 h under hydrothermal conditions. The product was isolated with a magnet, washed with ethanol and water several times, and dried at 50°C overnight to obtain the CHMSs.

Finally, MPS was used to introduce the hydrolysable group [—$Si(OCH_3)_3$] and unsaturated carbon–carbon double bonds onto the surface of the CHMSs.[20] The HMSs (0.3 g) were added to 60 mL of the ethanol–water mixed solvent (3 : 1 v/v), 2 mL of MPS was added dropwise, and then, the system was mechanically stirred at 65°C for 4 h under an $N_2$ atmosphere. After the reaction, the SCHMSs were obtained by magnetic separation, rinsed with ethanol, and dried.

### Synthesis of the TSCHMSs

Dual-responsive hollow microspheres were prepared as follows: 0.5 g of the NIPAM monomer and 0.075 g of the crosslinker, *N,N′*-methylene bisacrylamide, were dissolved in 45 mL of water and sonicated for 10 min. Then, the mixture was transferred into a three-necked flask equipped with a reflux denser and deoxygenized with nitrogen for 30 min. The SCHMSs (0.1 g) were added with mechanical stirring at 40°C. Subsequently, the suspension was heated to 70°C. At last, 1 mL of a 5 g/L potassium persulfate solution was rapidly dropped into the mixed system to initiate the polymerization, which was performed at 70°C for 12 h under nitrogen. The product was collected,

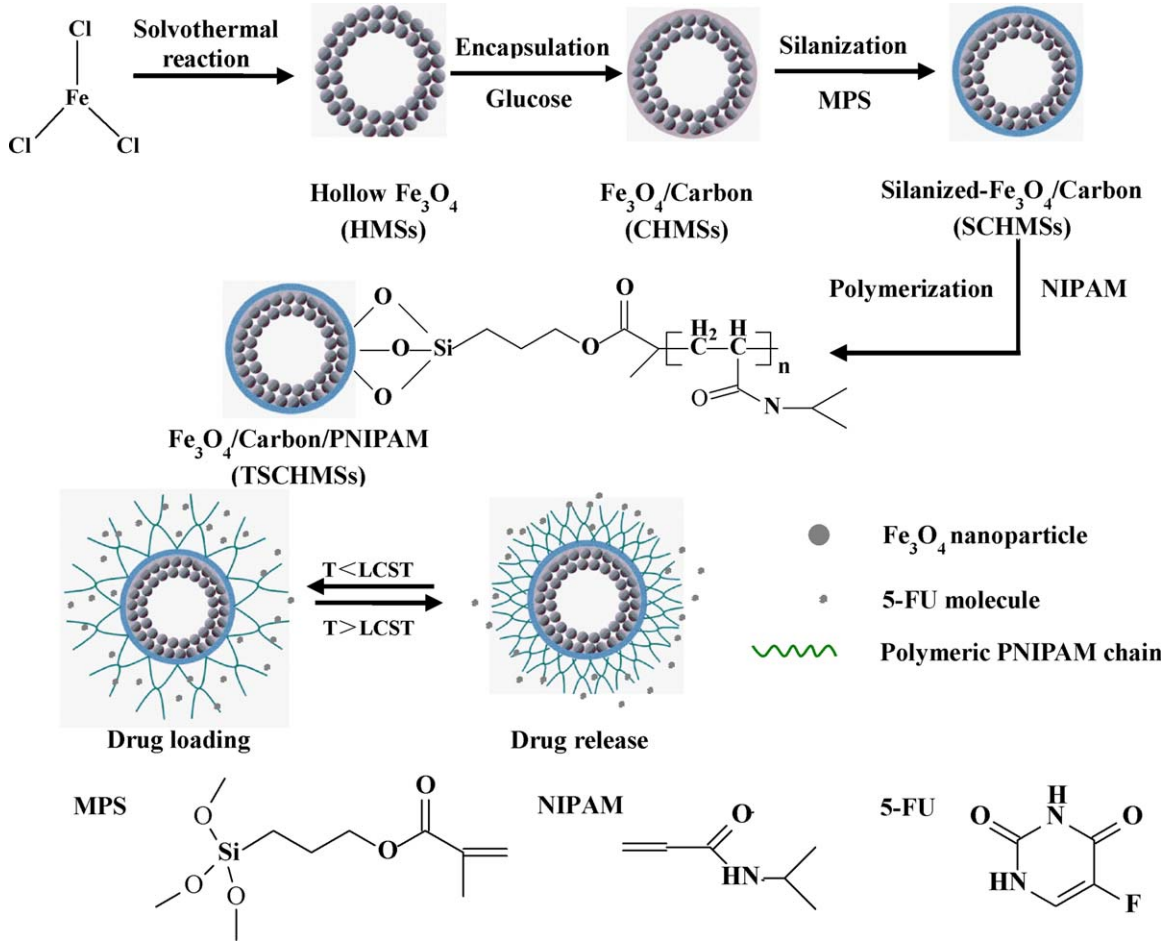


**Figure 1.** Schematic illustration of the synthesis, drug loading, and release of the hollow dual-responsive microspheres. T = temperature. [Color figure can be viewed in the online issue, which is available at wileyonlinelibrary.com.]

washed with ethanol three times to remove unreacted reagents, and dried.

### Loading and Release Behavior Test

The drug loading of 5-FU was carried out in a thermostatic oscillator at a rate of 160 rpm. In brief, 5-FU was dissolved in a PBS solution to prepare a 1 g/L solution. The TSCHMSs (200 mg) were suspended in 20 mL of 5-FU solution and allowed to shake in the oscillator at 25°C for 12 h. The drug-loading microspheres were collected by a magnet, washed with a PBS solution, and dried *in vacuo* overnight. Ultraviolet–visible spectrophotometry was used to estimate the drug-loading efficiency by analysis of the supernatant, which could be obtained by the following equation:[23]

$$\text{Drug-loading efficiency (mg/g)} = [(C_0 - C_t)/m] \times V \quad (1)$$

where $C_0$ and $C_t$ are the initial and ultimate concentrations of the drug (mg/L), respectively; $V$ is the volume of solution (L); and $m$ is the mass of the TSCHMSs (g).

The thermotriggered release behavior was evaluated by the immersion of 20 mg of drug-loading microspheres into 40 mL of a PBS solution at 35 and 50°C, separately. The release measurement was conducted in an oscillator. At specific time intervals, aliquots of the solutions were sucked up, and equivalent PBS was supplemented. The amount of release drug was determined by ultraviolet–visible spectrophotometry. Cumulative drug release ($F$) from the microspheres was obtained by the following formula:

$$F = (M_t/M_0) \times 100\% \quad (2)$$

where $M_t$ and $M_0$ are the cumulative release mass of the drug at time $t$ and the initial loaded drug content on the TSCHMSs (mg), respectively.

### Characterization and Measurements

The morphologies of the microspheres in the dried state were inspected with scanning electron microscopy (SEM; JSM-7001F) at an accelerating voltage of 10.0 kV and with transmission electron microscopy (TEM; JEOL, JEM 2100). Energy-dispersive X-ray spectroscopy (EDS; Bruker) was used to identify the element at a scanning voltage of 15.0 kV. The crystalline characteristics were measured with X-ray diffraction (XRD; DX-2700) with Cu K$\alpha_1$ radiation ($\lambda = 1.5406$ Å). The chemical compositions and stabilities were determined via thermogravimetry (TG; 209 F3, Netzsch) in an air atmosphere at a heating rate of 10°C/min. Fourier transform infrared (FTIR) spectroscopy (Tensor 27, Bruker) was used to characterize various functional groups on the surface of the microspheres. The magnetization

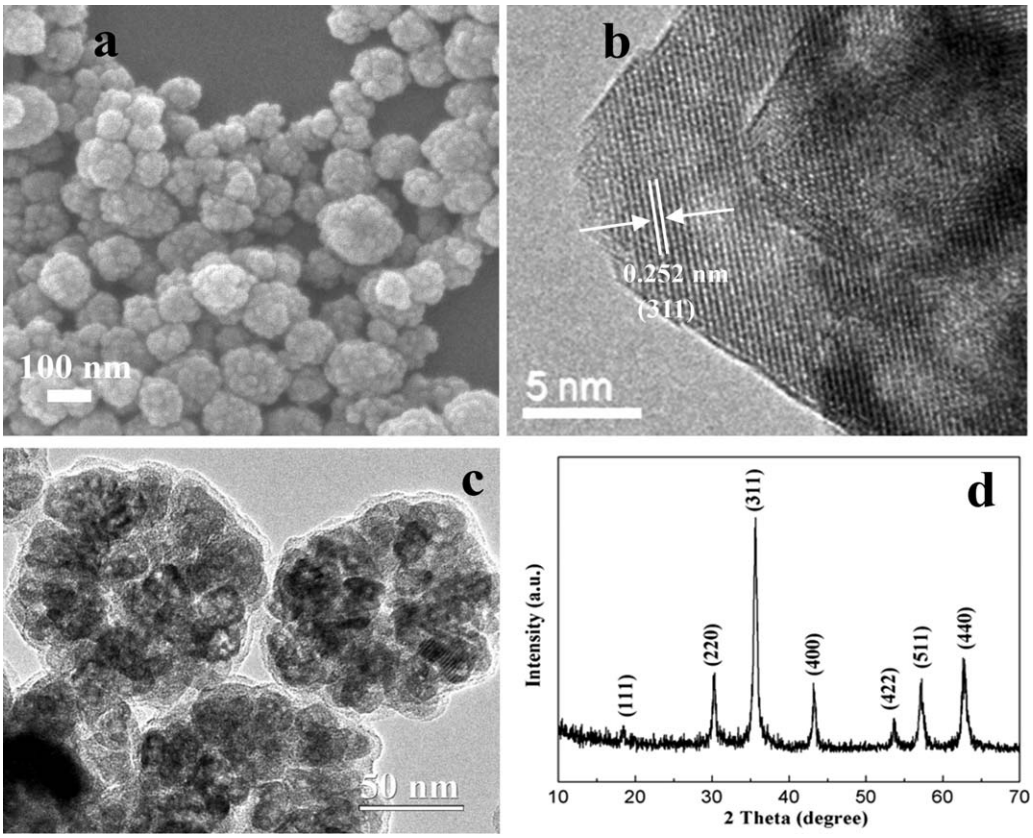


**Figure 2.** (a) SEM and (b) TEM images of HMSs and (c) TEM image and (d) XRD patterns of the obtained CHMSs.

in the applied magnetic field was performed by a vibrating sample magnetometer (Versalab, Quantum design) at 25°C. The properties of thermosensitivity were measured with a dynamic light scattering (DLS) instrument (Zetasizer Nano-ZS90, Malvern). The 5-FU loading and release properties were determined with an ultraviolet–visible spectrophotometer (U-3900, Hitachi) operated at 264 nm. A microscope equipped with a charge-coupled camera was introduced to measure the contact angle. Every droplet of water was 5 $\mu$L. Inductive heating was accomplished by the positioning of 1 g/L microsphere PBS dispersion in an alternating magnetic field; this was created by a high-frequency induction heater (SP-04C, 350A, Shenzhen, China).

## RESULTS AND DISCUSSION

### Synthesis and Characterization of the TSCHMSs

The SEM and TEM images were taken to give insight into the morphology and microstructure of the products at different stages. Figure 2(a) shows that the as-synthesized samples were spheres with a diameter around 100 nm in the dried state. It was clear that the microspheres consisted of multiple nanoparticles. To further demonstrate the pattern of the nanoparticles, a TEM image is given in Figure 2(b). The latticed spacing of 0.252 nm corresponded to the (311) planes of $Fe_3O_4$, which is identified in Figure 2(d). As shown in Figure 2(c), the hollow structure of the CHMSs was confirmed.[18] In addition, a carbon layer was consistently encapsulated around the HMSs to realize their space stabilization. The XRD patterns of the CHMSs [Figure 2(d)] exhibited diffraction peaks of $Fe_3O_4$ nanocrystals, which matched well to JCPDS No. 190629.[28] The diameter of $Fe_3O_4$ obtained by Scherrer's formula was estimated to be about 18.4 nm. However, there was no apparent diffraction peak of graphite in the XRD patterns; this suggested the amorphous nature of the carbon layer or difficulty in detecting the thin layer.

The morphological structures of the SCHMSs and TSCHMSs are shown in Figure 3(a,c), respectively. By silanization, the signal of Si appeared in the EDS spectrum [Figure 3(b)]; this demonstrated that the silane coupling agent was grafted onto the surface of CHMSs. After polymerization, the sizes of the TSCHMSs increased, and their surface became rougher because of the coating of the thermosensitive polymer. In addition, the N signal emerged in the EDS spectrum [Figure 3(d)]; this originated from the NIPAM monomer. After grafting, the average size of the microspheres increased slightly from 114 to 135 nm. These results further verify that the thermosensitive polymers were crosslinked around the surfaces of the SCHMSs.

To quantify the weight percentage of $Fe_3O_4$ and investigate the stability of the as-obtained samples, TG analysis was conducted. The TG curves for the HMSs, CHMSs, and SCHMSs are shown in Figure 4(a), and the corresponding differential TG curves are displayed in Figure 4(b). The HMSs had two apparent decomposition temperatures at 266 and 590°C separately; this led to a 4.82% total weight loss and showed a thermally stable nature. The first approximate 3.0% weight loss at 266°C was attributed to the decomposition of a few oligomers that were embedded in

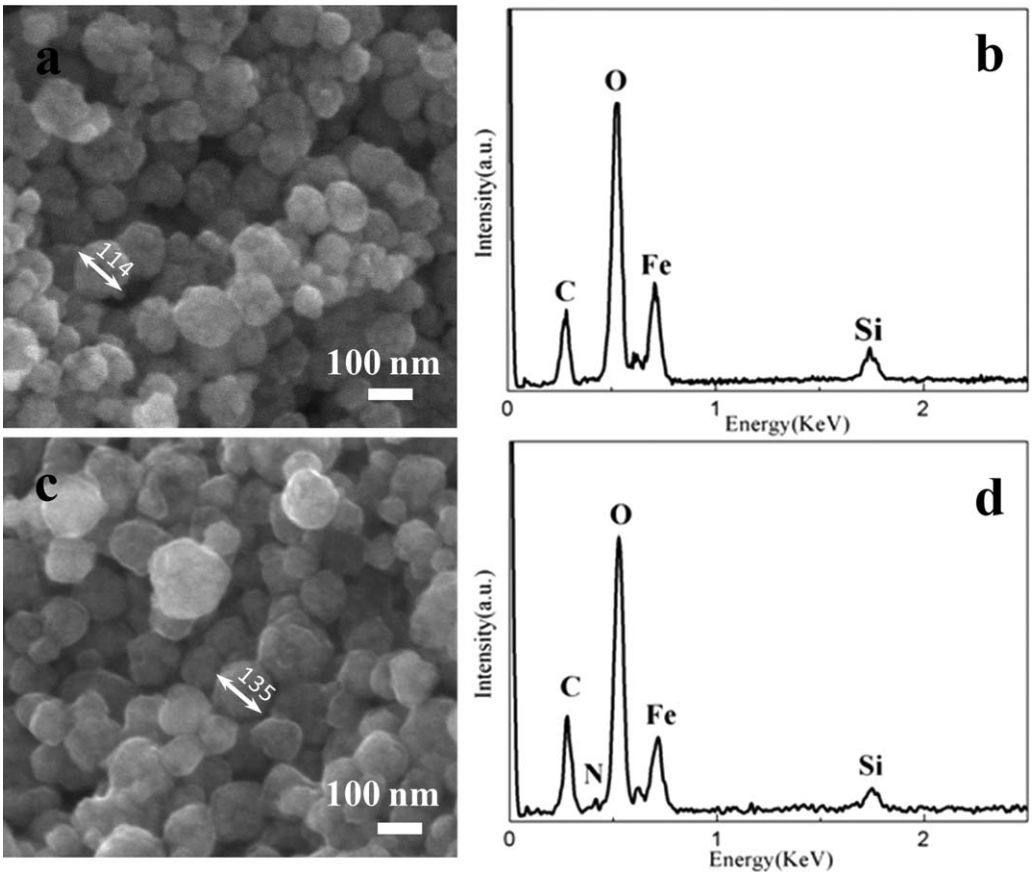


**Figure 3.** (a) SEM image and (b) EDS spectrum of the SCHMSs and (c) SEM image and (d) EDS spectrum of the TSCHMSs.

the MNPs. Because the solvent, ethylene glycol, could oligomerize in the solvothermal method at 200°C, the oligomers were produced along with the formation of the $Fe_3O_4$ hollows, although the decomposition occurring at 590°C may have been induced by the conversion of $Fe_3O_4$ nanoparticles to $Fe_2O_3$ nanoparticles. After carbon encapsulation, the weight loss of the CHMSs was increased by 14.41%, and the decomposition temperatures were extended to 316 and 614°C, respectively. The delay may have been caused by the previous decomposition of the carbon layer around the HMSs. Compared with the CHMSs, the SCHMSs had a 3.13% lower weight loss as a result of the pyrolysis of grafted MPS to $SiO_2$.[29] The formed $SiO_2$ adhered on the surface of the magnetic microspheres and further delayed the phase transformation of $Fe_3O_4$ nanoparticles to 664°C.

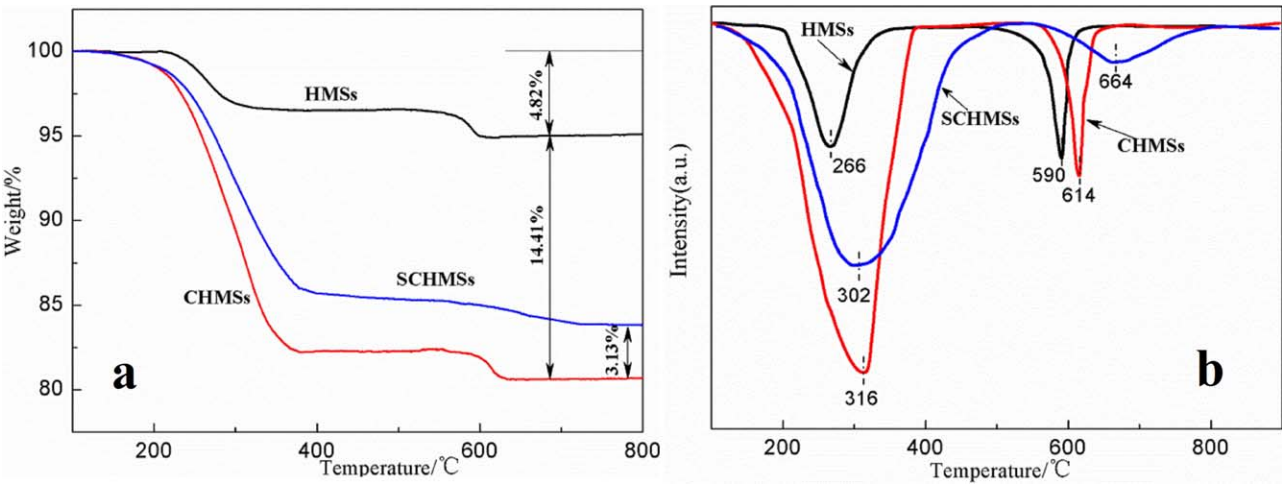


**Figure 4.** (a) TG and (b) differential TG curves of the as-synthesized HMSs, CHMSs, and SCHMSs. [Color figure can be viewed in the online issue, which is available at wileyonlinelibrary.com.]

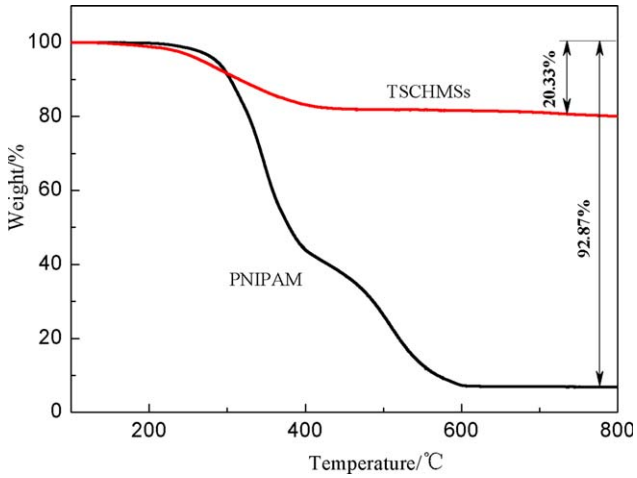


**Figure 5.** TG curves of the TSCHMSs and PNIPAM. [Color figure can be viewed in the online issue, which is available at wileyonlinelibrary.com.]

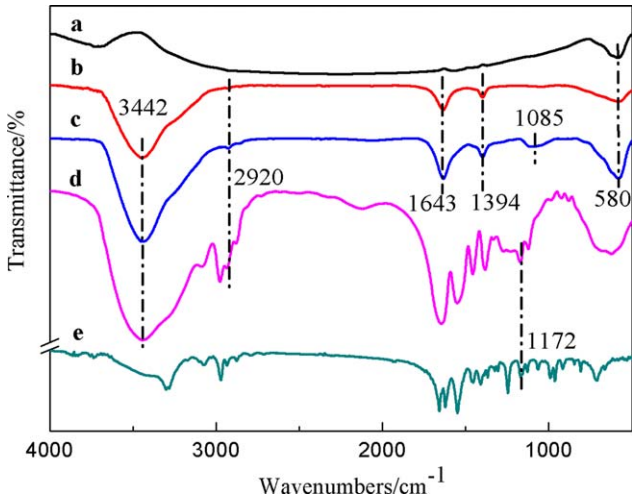


**Figure 6.** FTIR spectra of the (a) HMSs, (b) CHMSs, (c) SCHMSs, (d) TSCHMSs, and (e) NIPAM. [Color figure can be viewed in the online issue, which is available at wileyonlinelibrary.com.]

Figure 5 shows the TG curves of the TSCHMSs and thermosensitive polymer PNIPAM. The weight loss of PNIPAM increased rapidly from 300 to 600°C; this was ascribed to the thermal decomposition of the polymer. The weight losses of the SCHMSs [Figure 4(a)], TSCHMSs, and PNIPAM were 16.10, 20.33, and 92.87 wt %, respectively. Therefore, the grafting ratio of the polymer in the TSCHMSs ($x$) was 5.51 wt % and was obtained as follows:

$$x \times 92.87\% + (1-x) \times 16.10\% = 20.33\%$$

The previous differences illustrated that the SCHMSs, TSCHMSs, and PNIPAM were different from each other in thermal stability; this was caused by the grafting of the polymer onto the SCHMS cores.

To confirm the existence and kinds of surface groups, FTIR analyses were carried out on the HMSs, CHMSs, SCHMSs, TSCHMSs, and NIPAM, as shown in Figure 6. In the FTIR spectra of the HMSs [Figure 6(a)], the strong band at 580 $cm^{-1}$ corresponded to the Fe—O vibration. After carbon encapsulation, the spectra of the CHMSs [Figure 6(b)] displayed four new bands at 1394, 1643, 2920, and 3442 $cm^{-1}$; these were assigned to carboxyl O═C—O, C═O, C—H, and —OH groups, respectively. This demonstrated that the hydrothermal method not only realized carbon encapsulation but also functionalized the microspheres with abundant oxygen-containing groups. The weak band at 1085 $cm^{-1}$ [Figure 6(c)] was the vibration of the Si—O bond, which was derived from MPS. However, the desired unsaturated carbon–carbon bonds in the silane coupling agent coincided with the bands of the carboxyl groups from the CHMSs. As to the spectra of the TSCHMSs [Figure 6(d)], the characteristic bands of the —OH, C—H, and C═O stretching vibrations were still present, whereas the characteristic bands of the N—H groups originating from the thermosensitive polymer coincided with the same band. The band at 1172 $cm^{-1}$ was attributed to the skeleton stretching vibrations of C—C from isopropyl groups.[30] These results confirm that the TSCHMSs were synthesized with the thermosensitive polymer crosslinked on the surface.

### Thermosensitive Properties of the TSCHMSs

The temperature-induced scale variations of the TSCHMSs were studied by DLS, as given in Figure 7(a). When the temperature raised from 25 to 60°C, the hydrodynamic diameter underwent

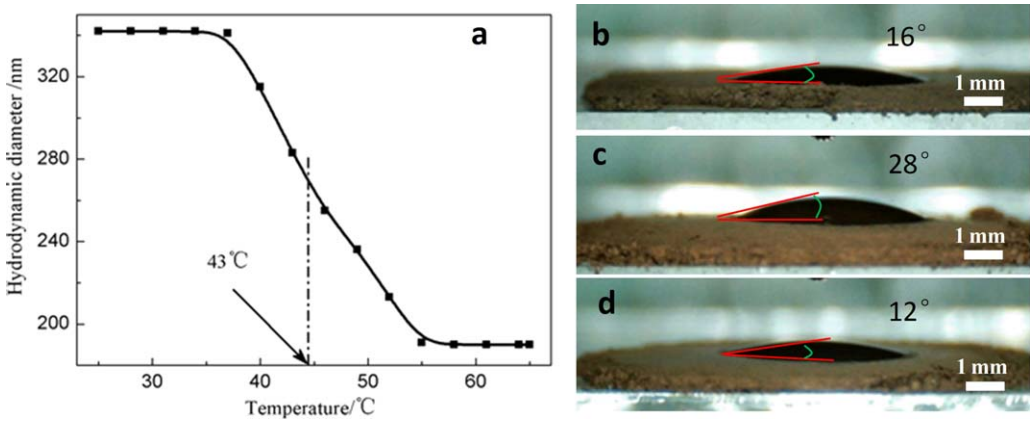


**Figure 7.** (a) DLS measurements of the TSCHMSs at different temperatures and (b–d) wettability of the CHMSs, SCHMSs, and TSCHMSs, respectively, at 25°C. [Color figure can be viewed in the online issue, which is available at wileyonlinelibrary.com.]

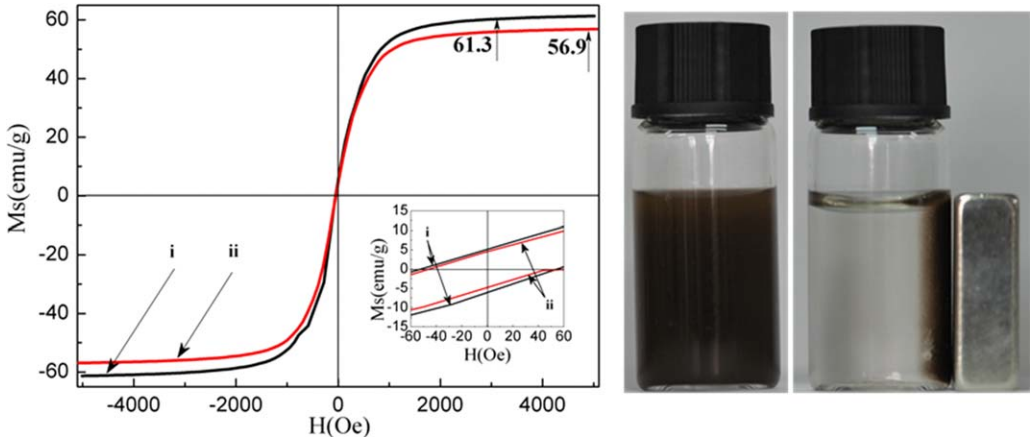


**Figure 8.** Magnetic hysteresis loops of the (i) HMSs and (ii) TSCHMSs and photograph of the TSCHMS suspension with a magnet. H = intensity of magnetic field. [Color figure can be viewed in the online issue, which is available at wileyonlinelibrary.com.]

a sharp decrease from 342 to 190 nm around 43°C. At room temperature (25°C), it was noticeable that the hydrodynamic diameter was about 200 nm larger than the average size determined by SEM and TEM (~100 nm). This was because DLS displayed the whole size, including the organic polymer swollen in the aqueous phase, whereas SEM and TEM showed the size in the dried state. Moreover, according to Figure 7(a), the TSCHMSs had a phase transition around 43°C and demonstrated typical temperature-responsive properties. This behavior resulted from the swelling and shrinking of the polymer layer at different temperatures. When the temperature was below LCST, the polymer layer was hydrophilic in the aqueous solution and existed in the swollen state. With increasing temperature to above LCST, the polymer layer became hydrophobic interaction. Water molecules were excluded away from the polymer chains, and this led to their contraction and a lower hydrodynamic diameter.[31]

In this study, LCST of the TSCHMSs was 43°C, 8°C higher than that of the PNIPAM polymer (35°C).[10] Similar results were obtained and discussed in our previous work,[20] in which we which selected carbon-encapsulated solid MNPs as cores and PNIPAM as a thermosensitive shell. The most possible explanation was the hydrophobicity–hydrophilicity balance of the composites on which the LCST mainly depended. Therefore, the wettability of the microspheres was studied by the measurement of their contact angles [Figure 7(b–d)]. The CHMSs were quite hydrophilic with a small contact angle of 16°; this was attributed to the existence of multiple functional groups on the surface of the carbon shell (confirmed by FTIR spectrum). After silanization, the introduction of the vinyl group is bound to reduce their hydrophobicity, leading to a higher contact angel of 28°. After grafting the thermosensitive polymer on the surface, the hydrophilicity increases again, with a lower contact angle of 12°. As reported in the previous literature, the contact angle of the PNIPAM microspheres is about 83°,[32] which is much higher than that of TSCHMSs. It suggests that TSCHMSs have better hydrophilicity, resulting in a higher LCST.

### Magnetic Properties of the TSCHMSs

As for medical application, it is significant that functionalized microspheres maintain their magnetism after silanization and polymerization. The magnetism was also confirmed by a magnet, as displayed in the photograph in Figure 8. In addition, Figure 8 shows the magnetic hysteresis loops of the HMSs and TSCHMSs at 25°C. After grafting, the saturated magnetization ($M_s$) decreased from 61.3 to 56.9 emu/g as a result of the decrease in the HMS content in the TSCHMSs. Also, both of the curves nearly intersected with the original point, demonstrating their almost no coercivity and remanence and revealing

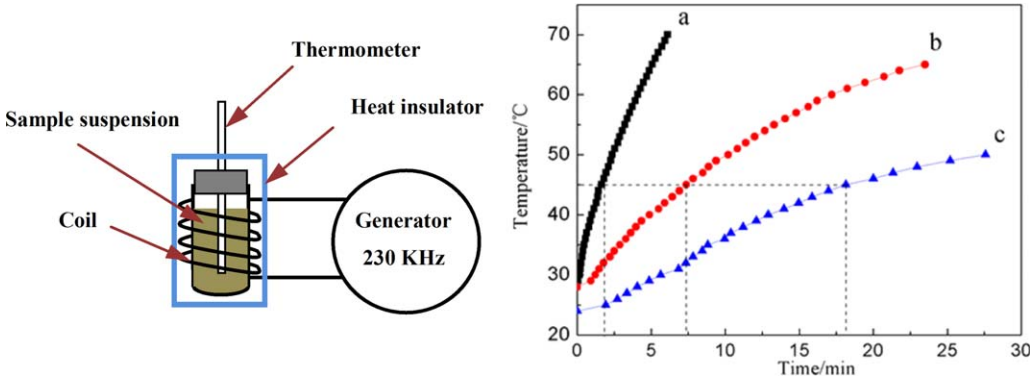


**Figure 9.** Experimental setup for the inducting heating and curves of the temperature of the medium versus time for the (a) HMSs, (b) CHMSs, and (c) TSCHMSs. [Color figure can be viewed in the online issue, which is available at wileyonlinelibrary.com.]

**Table I.** SAR of the As-Synthesized Microspheres in Comparison with Other Literature Values

| Hyperthermia thermoseeds | $M_s$ (emu/g) | Calculated SAR (W/g) | Normalized SAR (W/g) | Reference |
|---|---|---|---|---|
| HMSs | 61.3 | 2732 | 1412 | This study |
| CHMSs | 57.6 | 739 | 382 | This study |
| TSCHMSs | 56.9 | 466 | 240 | This study |
| $Fe_3O_4$/carbon/PNIAPM microspheres | 13.8 | 149 | 77 | 20 |
| $Fe_3O_4$ nanoparticles | — | — | 40 | 36 |
| $Fe_3O_4$/PEG nanoparticles | 51.0 | — | 367 | 34 |

their superparamagnetic nature. This character could keep their stability in the dispersions so as to conveniently transport in the practical application.[33]

### Inductive Heating Properties of the As-Synthesized Microspheres

An inductive heating test was performed to evaluate the efficiency of the microspheres as hyperthermia mediators. An inductive magnetic field of 230 kHz and 290 Oe was produced by a high-frequency induction heater. Figure 9 shows the experimental setup and temperature of the medium versus time curves of the HMSs, CHMSs, and TSCHMSs. We found that when they were placed in the inductive magnetic field for 2, 7.5, and 18 min, the temperature of suspension for the HMSs, CHMSs, and TSCHMSs reached 45°C separately. A significant extension of the heating time was observed for samples with the carbon and polymer coating. Similar results were obtained in previous studies; this confirmed that the coated polymer could change the magnetic properties.[34] The heat introduced by the MNPs under an alternative magnetic field was mainly ascribed to Brownian relaxation and Néel relaxation.

In an external alternative magnetic field, the tumor issue containing the thermoseeds increased its temperature to 41–46°C. The tumor cells could be killed by the heat, and this accomplished hyperthermia.[35] This demonstrated that the TSCHMSs have the potential for hyperthermia treatment. In addition, to better understand the inductive heating properties, the specific adsorption (SAR) was introduced; this was obtained with the following equation:[21]

$$\mathrm{SAR} = C_p(dT/dt)(M/m) \quad (3)$$

$$M = m_{\mathrm{PBS}} + m_{\mathrm{magnetic\ \ microspheres}} \quad (4)$$

where $C_p$ is 4.186 J $g^{-1}$ $K^{-1}$, $dT/dt$ is the slope of the temperature versus time curve, $m$ is the mass of the magnetic content and $M$ is the total mass of the PBS solution and the magnetic content. The SAR values for the HMSs, CHMSs, and TSCHMSs were 2732, 739, and 466 W/g, respectively. To obtain an exact comparison with the literature data, the SAR was normalized to 1 MHz and 100 Oe because it was proportional to the frequency and the square of the field strength. Table I summarizes the SARs of several thermoseeds and the as-synthesized microspheres. It was evident that the microspheres with high $M_s$ values led to a high SAR. Exceptionally, although $M_s$ of $Fe_3O_4$/PEG nanoparticles was 51.0 emu/g; this was lower than that of the TSCHMSs. It had a higher normalized SAR. This was attributed to the smaller diameter. A weakened SAR with increasing thickness of the surface coating was observed, and this was ascribed to the decreased Brownian loss.[34] The TSCHMSs with an SAR of 240 w/g were comparable to other magnetic microspheres. These showed potential for hyperthermia treatment.

### Interactions Between NIPAM and 5-FU

Because the 5-FU structure contained a fluorine atom, its electronegativity increased, and it had an electron-withdrawing effect. This made it easier to form hydrogen bonds with hydrogen atoms in NIPAM. Moreover, there was a negatively charged amide oxygen in the NIPAM structure; this also tended to form hydrogen bonds with the hydrogen atoms in 5-FU. Therefore, 5-FU could be loaded by the thermoresponsive polymer. In this

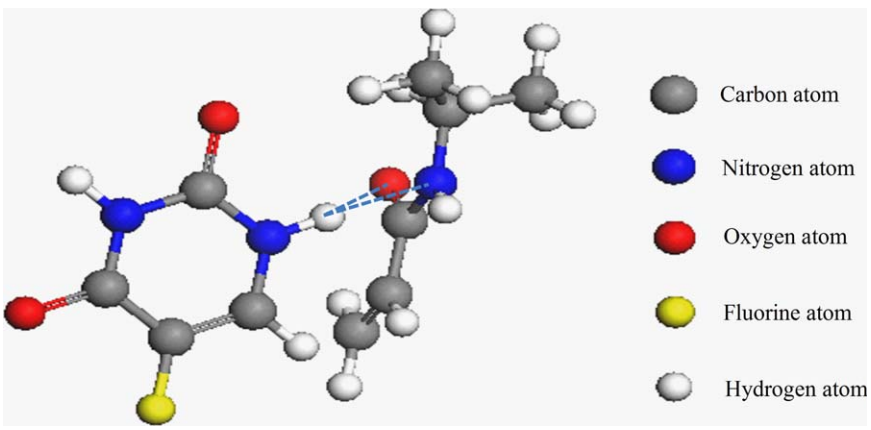


**Figure 10.** Optimized system of the template-functional monomer 5-FU/NIPAM. [Color figure can be viewed in the online issue, which is available at wileyonlinelibrary.com.]

**Table II.** Total Energy of 5-FU, NIPAM, and 5-FU/NIPAM

| Molecule | 5-FU | NIPAM | 5-FU/NIPAM |
|---|---|---|---|
| Total energy (Ha)[a] | −514.16966 | −365.232338 | −879.428514 |

[a] 1 Ha = 2625.552 kJ/mol.

study, the NIPAM, 5-FU, and 5-FU/NIPAM complex were optimized and calculated by general gonadotropic activity/Becke, Lee, Parr and Yang (GGA/BLYP) and double numerical plus polarization (DNP) level of theory. All of the calculations were carried out the application of the Dmol3 program in Material Studio (Accelrys). The results are displayed in Figure 10 and Table II. The binding energy of 5-FU/NIPAM was calculated as follows:

$$\Delta E = E_{5-FU/NIPAM} - E_{5-FU} - E_{NIPAM} = -0.016516 \text{ Ha} = -43.32 \text{ kJ/mol}$$

where $E$ is the total energy and $\Delta E$ is the binding energy.

Such a negative value revealed that the interaction force was attractive. This further illustrated that the hybrid microspheres with a PNIAM layer were used as a drug carrier for 5-FU.

### *In Vitro* Controlled Release

The drug-loading efficiency of the TSCHMSs (30.3 mg/g) was obtained by analysis of the supernatant of the microsphere loading to saturation with the model drug 5-FU. The thermotriggered release behavior was evaluated at 35 and 50°C; this corresponded to the temperature below and above their LCST, respectively. The release profiles exhibited marked differences at different release temperatures, as shown in Figure 11. At 35°C, 18.8% 5-FU was released from the microspheres. In contrast, the microspheres showed a fast and higher release rate at 50°C, and 36.2% of 5-FU was released. This was nearly double that for the temperature below LCST. Thus, the drug release depended on the temperature of the medium, by which the thermotriggered release could be realized. The release mechanisms of these TSCHMSs mainly relied on the dehydration and water absorption properties of the thermosensitive polymer around LCST; this is illustrated in Figure 1. Because 5-FU was hydrophilic, it approached the polymer layer motivated by electrostatic forces below LCST. When the temperature was higher than LCST, the polymer chains shrank to a dehydrated status, and the hydrophobic effect sped up the release of 5-FU.[23]

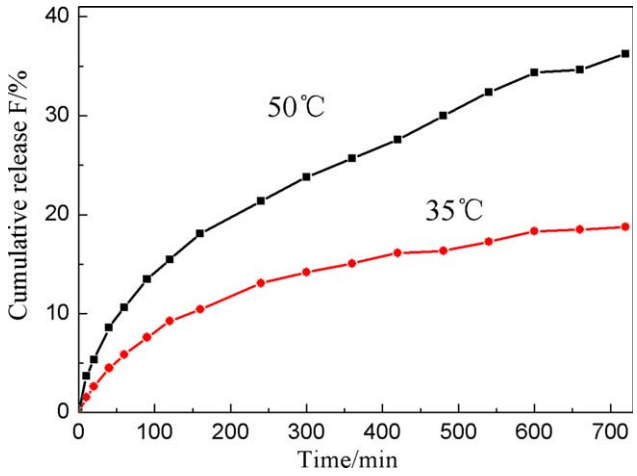


**Figure 11.** Release profile of the TSCHMSs at 35 and 50°C. [Color figure can be viewed in the online issue, which is available at wileyonlinelibrary.com.]

### Drug-Release Kinetics

To further understand the drug-release kinetics, the Ritger-Peppas model was used to fit the previous release profiles:[21]

$$F = kt^n \quad (5)$$

where $F$ is the fractional drug release into the dissolution medium, $k$ is a rate constant, and $n$ is the diffusional exponent. According to the linear fit of ln $F$ versus ln $t$, $n$ and $k$ were obtained. When $n$ is 0.5, Fickian diffusion determines the release. When $n = 1$, the release is controlled by the relaxation of the polymer chains. When $0.5 < n < 1$, an anomalous, non-Fickian drug release occured.[21] According to the fitting results, the $n$ values in this work were 0.57 and 0.53 at 35 and 50°C, respectively; this indicated an anomalous (non-Fickian) or quasi-Fickian mechanism for drug release. The quasi-Fickian mechanism was attributed to the combined release through the diffusion of the drug and the relaxation of the polymer. These outcomes verified that TSCHMSs had outstanding drug loading and thermotriggered release ability for 5-FU.

## CONCLUSIONS

In summary, we present a new approach for preparing thermoresponsive magnetic microspheres with hollow $Fe_3O_4$ particles by surface radical polymerization for the controlled release of 5-FU. A carbon nanomaterial was used as a steric stabilizer for $Fe_3O_4$ nanoparticles and as a supporter for the polymer. DLS measurements revealed that the hybrid microspheres exhibited an obvious thermosensitivity, whose LCST occurred around 43°C. Inductive heating studies showed that the microspheres had a specific absorption rate of 240 W/g and showed potential for hyperthermia treatment. 5-FU was loaded into the microspheres and released from them through the control of the temperature with applied magnetic field induction. The hollow dual-responsive microspheres showed great promise for being a good drug carrier in the biomedical field.

## ACKNOWLEDGMENTS

This work was financially supported by the Postgraduate Innovation Program of Shanxi Province (contract grant sponsor 20143005), the Postgraduate Innovation Foundation of Taiyuan University of Technology (contract grant sponsor B2014015), the Shanxi Provincial Key Innovative Research Team in Science and Technology (contract grant sponsor 2012041011), the International Science and Technology Cooperation Program of China (contract grant sponsor 2012DFR50460), and the Shanxi Scholarship Council of China through a research project (contract grant sponsor 2012-038).

## REFERENCES


1. Thevenot, J.; Oliveira, H.; Sandre, O.; Lecommandoux, S. *Chem. Soc. Rev.* **2013**, *42*, 7099.
2. Jaiswal, M. K.; De, M.; Chou, S. S.; Vasavada, S.; Bleher, R.; Prasad, P. V.; Bahadur, D.; Dravid, V. P. *ACS Appl. Mater. Interfaces* **2014**, *6*, 6237.
3. Wang, H.; Yang, J.; Li, Y.; Sun, L.; Liu, W. *J. Mater. Chem. B* **2013**, *1*, 43.
4. Murali, R.; Vidhya, P.; Thanikaivelan, P. *Carbohydr. Polym.* **2014**, *110*, 440.
5. Coughlan, D. C.; Corrigan, O. I. *Int. J. Pharm.* **2006**, *313*, 163.
6. Sharifi, I.; Shokrollahi, H.; Amiri, S. *J. Magn. Magn. Mater.* **2012**, *324*, 903.
7. Laurent, S.; Dutz, S.; Hafeli, U. O.; Mahmoudi, M. *Adv. Colloid Interface Sci.* **2011**, *166*, 8.
8. Laurenti, M.; Guardia, P.; Contreras-Caceres, R.; Perez-Juste, J.; Fernandez-Barbero, A.; Lopez-Cabarcos, E.; Rubio-Retama, J. *Langmuir* **2011**, *27*, 10484.
9. Purushotham, S.; Ramanujan, R. V. *Acta Biomater.* **2010**, *6*, 502.
10. Rubio-Retama, J.; Zafeiropoulos, N. E.; Serafinelli, C.; Rojas-Reyna, R.; Voit, B.; Lopez-Cabarcos, E.; Stamm, M. *Langmuir* **2007**, *23*, 10280.
11. Deng, Y. H.; Yang, W. L.; Wang, C. C.; Fu, S. K. *Adv. Mater.* **2003**, *15*, 1729.
12. Chen, D.; Ji, G.; Ma, Y.; Lee, J. Y.; Lu, J. *ACS Appl. Mater. Interfaces* **2011**, *3*, 3078.
13. Shin, J.; Anisur, R. M.; Ko, M. K.; Im, G. H.; Lee, J. H.; Lee, I. S. *Angew. Chem. Int. Ed.* **2009**, *48*, 321.
14. Cheng, K.; Peng, S.; Xu, C.; Sun, S. *J. Am. Chem. Soc.* **2009**, *131*, 10637.
15. Kawashita, M.; Sadaoka, K.; Kokubo, T.; Saito, T.; Takano, M.; Araki, N.; Hiraoka, M. *J. Mater. Sci. Mater. Med.* **2006**, *17*, 605.
16. Wei, J.; Ju, X. J.; Zou, X. Y.; Xie, R.; Wang, W.; Liu, Y. M.; Chu, L. Y. *Adv. Funct. Mater.* **2014**, *24*, 3312.
17. Zhang, Y.; Xu, S.; Luo, Y.; Pan, S.; Ding, H.; Li, G. *J. Mater. Chem.* **2011**, *21*, 3664.
18. Yu, D.; Sun, X.; Zou, J.; Wang, Z.; Wang, F.; Tang, K. *J. Phys. Chem. B* **2006**, *110*, 21667.
19. Pan, J.; Yin, Y.; Wu, R.; Dai, X.; Dai, J.; Gao, L. *J. Ind. Eng. Chem.* **2015**, *25*, 321.
20. Chen, L.; Li, L.; Zhang, H.; Liu, W.; Yang, Y.; Liu, X.; Xu, B. *RSC Adv.* **2014**, *4*, 46806.
21. Chen, M. L.; He, Y. J.; Chen, X. W.; Wang, J. H. *Langmuir* **2012**, *28*, 16469.
22. Fan, X.; Jiao, G.; Gao, L.; Jin, P.; Li, X. *J. Mater. Chem. B* **2013**, *1*, 2658.
23. Anirudhan, T. S.; Mohan, A. M. *RSC Adv.* **2014**, *4*, 12109.
24. Spanakis, M.; Bouropoulos, N.; Theodoropoulos, D.; Sygellou, L.; Ewart, S.; Moschovi, A. M.; Siokou, A.; Niopas, I.; Kachrimanis, K.; Nikolakis, V.; Cox, P. A.; Vizirianakis, I. S.; Fatouros, D. G. *Nanomedicine* **2014**, *10*, 197.
25. Zhu, K.; Ye, T.; Liu, J.; Peng, Z.; Xu, S.; Lei, J.; Deng, H.; Li, B. *Int. J. Pharm.* **2013**, *441*, 721.
26. Qi, D.; Lu, J.; Deng, C.; Zhang, X. *J. Phys. Chem. C* **2009**, *113*, 15854.
27. Liu, Y.; Wang, Y.; Zhou, S.; Lou, S.; Yuan, L.; Gao, T.; Wu, X.; Shi, X.; Wang, K. *ACS Appl. Mater. Interfaces* **2012**, *4*, 4913.
28. Kong, L.; Lu, X.; Bian, X.; Zhang, W.; Wang, C. *ACS Appl. Mater. Interfaces* **2010**, *3*, 35.
29. Duan, F.; Chen, C.; Chen, L.; Sun, Y.; Wang, Y.; Yang, Y.; Liu, X.; Qin, Y. *Ind. Eng. Chem. Res.* **2014**, *53*, 14291.
30. Tsuboi, Y.; Nishino, M.; Sasaki, T.; Kitamura, N. *J. Phys. Chem. B* **2005**, *109*, 7033.
31. Otake, K.; Inomata, H.; Konno, M.; Saito, S. *Macromolecules* **1990**, *23*, 283.
32. Plunkett, K. N.; Zhu, X.; Moore, J. S.; Leckband, D. E. *Langmuir* **2006**, *22*, 4259.
33. Oh, J. K.; Park, J. M. *Prog. Polym. Sci.* **2011**, *36*, 168.
34. Liu, X. L.; Fan, H. M.; Yi, J. B.; Yang, Y.; Choo, E. S. G.; Xue, J. M.; Fan, D. D.; Ding, J. *J. Mater. Chem.* **2012**, *22*, 8235.
35. Yang, J. K.; Yu, J. H.; Kim, J.; Choa, Y. H. *Mater. Sci. Eng. A* **2007**, *449*, 477.
36. Drake, P.; Cho, H. J.; Shih, P. S.; Kao, C. H.; Lee, K. F.; Kuo, C. H.; Lin, X. Z.; Lin, Y. J. *J. Mater. Chem.* **2007**, *17*, 4914.